Tectonics

RESEARCH ARTICLE
10.1029/2017TC004878

Key Points:
- Three thermal events: (1) Triassic-Early Jurassic cooling and exhumation, (2) Late Jurassic-Cretaceous quiescence, and (3) rapid
- Block tilting of the Chatkal-Kurama terrane identified by the geospatial relationship of the thermochronological data
- The integration of the data from this study with published data from the Tian Shan, to produce an exhumation model for the Tian Shan

Supporting Information:
- Supporting Information S1
- Table S1
- Table S2

Correspondence to:
G. Jepson,
gilby.jepson@adelaide.edu.au

Citation:
Jepson, G., Glorie, S., Konopelko, D., Gillespie, J., Danišík, M., Mirkamalov, R., Mamadjanov, Y., & Collins, A. S. (2018). Low-temperature thermochronology of the Chatkal-Kurama terrane (Uzbekistan-Tajikistan): Insights into the Meso-Cenozoic thermal history of the western Tian Shan. *Tectonics*, *37*. https://doi.org/10.1029/2017TC004878

Received 1 NOV 2017
Accepted 12 SEP 2018
Accepted article online 25 SEP 2018

Low-Temperature Thermochronology of the Chatkal-Kurama Terrane (Uzbekistan-Tajikistan): Insights Into the Meso-Cenozoic Thermal History of the Western Tian Shan

Gilby Jepson[1], Stijn Glorie[1], Dmitry Konopelko[2,3], Jack Gillespie[1], Martin Danišík[4], Rustam Mirkamalov[5], Yunus Mamadjanov[6,7], and Alan S. Collins[1]

[1]Centre for Tectonics, Resources, and Exploration (TRaX), Department of Earth Sciences, The University of Adelaide, Adelaide, Australia, [2]Department of Geology and Geophysics, Saint Petersburg State University, Saint Petersburg, Russia, [3]Department of Geology and Geophysics, Novosibirsk State University, Novosibirsk, Russia, [4]John de Laeter Centre, TIGeR, School of Earth and Planetary Sciences, Curtin University, Perth, Australia, [5]State Committee of the Republic of Uzbekistan on Geology and Mineral Resources, Tashkent, Uzbekistan, [6]Institute of Geology, Earthquake Engineering and Seismology, Academy of Sciences of the Republic of Tajikistan, Dushanbe, Tajikistan, [7]Research Center for Ecology and Environment of Central Asia (Dushanbe), Chinese Academy of Sciences-Tajik Academy of Sciences, Dushanbe, Tajikistan

Abstract The Chatkal-Kurama terrane represents a key region in understanding the tectonic evolution of the western Tian Shan. In this contribution, we present new thermochronological data (zircon [U-Th-Sm]/He, apatite fission track, and apatite [U-Th-Sm]/He) and the associated thermal history models for 30 igneous samples from the Chatkal-Kurama terrane within Uzbekistan and Tajikistan (west of the Talas-Fergana Fault) and integrate our data with published data from the central Tian Shan (east of the Talas-Fergana Fault). The Chatkal-Kurama terrane experienced a phase of rapid cooling during the Triassic-Jurassic at ca. 225–190 Ma, which we interpret as a far-field response to the closure of the Palaeo-Asian Ocean or the accretion of the Qiangtang terrane on to the Eurasian margin. In the Late Jurassic to the Early Cretaceous, the Chatkal-Kurama terrane experienced a period of tectonic stability and denudation, before transitioning into a period of marine incursions of the Paratethys Sea. In contrast, fast cooling is recorded for the Kyrgyz central Tian Shan to the east of the Talas-Fergana Fault. The differing thermal histories at either side of the Talas-Fergana Fault suggest that the fault induced a topographic divide during the Late Jurassic-Early Cretaceous, with high relief in the east (Kyrgyz Tian Shan) and low relief to the west (Uzbek-Tajik Tian Shan). Finally, the Chatkal-Kurama terrane experienced renewed tectonic activity since ca. 30 Ma, related with the distant India-Eurasia collision and Pamir indentation. The Cenozoic reactivation induced crustal tilting of the Chatkal-Kurama terrane, progressively exposing deeper rocks to the southwest.

Plain Language Summary The Chatkal-Kurama terrane is the westernmost extent of the Tian Shan and one of the largest intracontinental mountain ranges in the world. The classical view of the plate tectonic paradigm implies that the majority of mountain building occurs at the margins of tectonic plates. Major ranges such as the Andes, the Himalaya, and the Rocky Mountains all form along the boundaries between major tectonic plates. However, the existence of major mountain ranges far from any modern plate boundary, such as the Tian Shan in Central Asia, forces us to consider how these intracontinental systems fit within the Earth system. These areas represent a unique challenge due to the complex nature of the tectonics, featuring multiple phases of deformation in response to far-field stress propagated from the plate margins into the continental interior. By using thermochronology in an intracontinental setting, such as the Chatkal-Kurama terrane, we aim to explore this complicated cooling history of the mountain ranges in this area and how that relates to the mountain growth in an intracontinental setting.

1. Introduction

Central Asia hosts one of the largest active intracontinental mountain belts in the world, the Tian Shan (Cawood et al., 2009). The Tian Shan is a vast mountain system that developed throughout the Mesozoic to Cenozoic as a response to tectonic forces at the distant Eurasian continental margins and has long been studied to understand the far-field effects of continental collision (e.g., Allen et al., 1991; Hendrix et al., 1992; Jolivet et al., 2013). A number of studies have applied thermochronological techniques throughout the Tian Shan in order to constrain the timing and extent of intracontinental deformation (e.g., Bande,

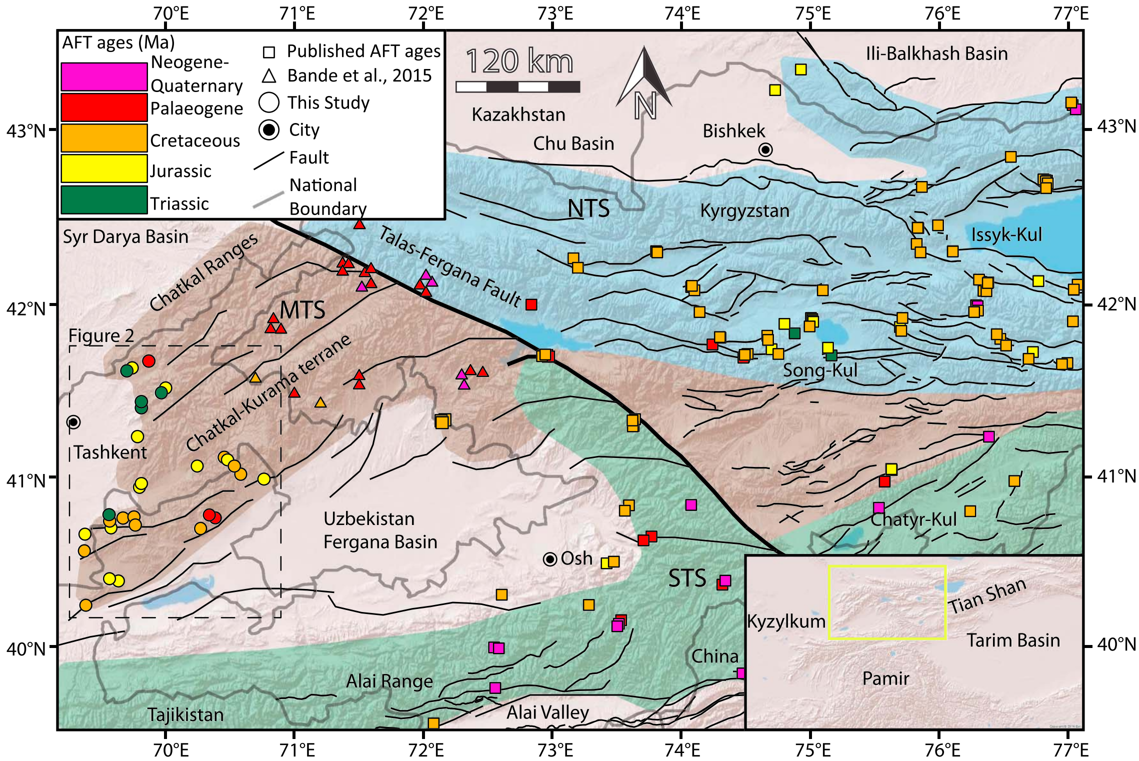

Figure 1. A shaded relief map of the western extent of the Tian Shan displaying published Mesozoic apatite fission track (AFT) ages for the region (color coded following AFT central ages). Circle symbols represent sample location for data obtained in this study, and triangles represent locations for data obtained by Bande, Sobel, Mikolaichuk, and Torres (2017; both to the west or in close proximity to the Talas-Fergana fault). Square symbols represent locations for published AFT ages from Sobel, Chen, et al. (2006), Sobel, Oskin, et al. (2006), Glorie et al. (2010), De Grave et al. (2013), Macaulay et al. (2014), De Pelsmaeker et al. (2015), Käßner, Ratschbacher, Pfänder, et al. (2017), Bande, Sobel, Mikolaichuk, Schmidt, et al. (2017), and Nachtergaele et al. (2018). The northern Tian Shan is denoted by NTS (shaded blue), the middle Tian Shan by MTS (shaded brown), and the South Tian Shan by STS (shaded green).

Sobel, Mikolaichuk, & Torres, 2017; De Grave et al., 2011; Glorie et al., 2011; Glorie & De Grave 2016; Sobel, Oskin, et al., 2006; Macaulay et al., 2014).

These studies demonstrated that following the final closure of the Palaeo-Asian (or Turkestan) Ocean and amalgamation of the terranes in the late Paleozoic, the Tian Shan experienced several major periods of cooling during the Mesozoic to Cenozoic. During the Mesozoic, distinct cooling events have been interpreted as related with exhumation in response to a number of Cimmerian collisions (e.g., the collisions of Qiangtang, Lhasa, and Karakorum with Eurasia; De Grave et al., 2013; Dumitru et al., 2001; De Pelsmaeker et al., 2015; Gillespie et al., 2017; Glorie & De Grave 2016; Jolivet et al., 2013; Käßner, Ratschbacher, Jonckheere, et al., 2017). The subsequent Cenozoic collision of India with Eurasia not only generated the Himalayas and the uplift of the Tibetan Plateau but is also thought to have driven uplift and deformation in the Asian continental interior, including the Tian Shan and other intracontinental mountain ranges (e.g., Bouilhol et al., 2013; Clift et al., 2002; Molnar & Tapponnier, 1975). Cenozoic cooling and exhumation is mainly recorded in close vicinity to major faults within the Tian Shan (e.g., Bande, Sobel, Mikolaichuk, & Torres, 2017; De Grave et al., 2012; Glorie et al., 2011; Glorie & De Grave 2016; Macaulay et al., 2014). While the thermochronology of most of the central Tian Shan (within Kyrgyzstan and China, to the east of the Talas Fergana Fault) has been extensively studied (Figure 1), such studies currently do not account for the western-most expression of the Tian Shan. A recent study by Bande, Sobel, Mikolaichuk, and Torres (2017) investigated the thermochronology of the Kyrgyz Chatkal ranges (Figure 1) and obtained mainly Cenozoic cooling ages (ca. 50–15 Ma), reflecting exhumation as a response to the indentation of the Pamir terrane. In this study, we apply low-temperature thermochronology to the Chatkal-Kurama terrane within western Uzbekistan and northern Tajikistan (west of the area studied by Bande, Sobel, Mikolaichuk, & Torres, 2017), plugging a critical gap in the thermochronological coverage of the region and developing a more complete picture of the thermal history of the western Tian Shan.

2. Geological Background

The ancestral Tian Shan formed in the late Paleozoic during the closure of the Palaeo-Asian Ocean and the subsequent collision of the Tarim Precambrian microcontinent with the southern margin of the early Paleozoic Kazakhstan continent (e.g., Biske & Seltmann, 2010; Burtman, 2015; Windley et al., 2007; Xiao et al., 2013). The western part of the Tian Shan (within Tajikistan, Uzbekistan, Kyrgyzstan, and Kazakhstan) is traditionally subdivided into three major tectonic terranes: (1) the Northern Tian Shan, representing the deformed margin of the Palaeo-Kazakhstan microcontinent; (2) the Middle Tian Shan, composed of a Precambrian microcontinental sliver and a superimposed island arc; and (3) the Southern Tian Shan, a late Paleozoic fold-and-thrust belt (Figure 1; Biske & Seltmann, 2010; Burtman, 2015). These east-west trending linear terranes are cut by the north-west trending Talas-Fergana Fault (TFF) with a total dextral offset of ~200 km (Figure 1; Burtman et al., 1996).

Our study area, the Chatkal-Kurama terrane, forms part of the Middle Tian Shan that is exposed west of the TFF (Figure 1; e.g., Windley et al., 2007). The Chatkal-Kurama terrane formed due to the accretion of an island arc (locally known as the Chatkal Arc) onto the passive southern margin of the Palaeo-Kazakhstan during the Late Ordovician (Alexeiev et al., 2016). This accretion caused the Chatkal arc to become the southern active margin of the Palaeo-Kazakhstan continent during the Late Silurian-Early Devonian, resulting in the generation of thick supra-subduction magmatic series (Dolgopolova et al., 2017; Konopelko, Seltmann, et al., 2017). During the Middle Devonian-Early Carboniferous, subduction halted and was followed by the deposition of carbonate sediments in a passive margin or transform fault environment, which were subsequently uplifted and eroded (Dolgopolova et al., 2017).

Subduction under the southern margin of the Chatkal-Kurama terrane resumed in the Early to Middle Carboniferous, generating voluminous Andean-type intrusions and volcanics. This magmatic series, with ages in the range of ca. 320–300 Ma, comprise the majority of the Chatkal-Kurama terrane (Figure 2; Dolgopolova et al., 2017; Konopelko, Seltmann, et al., 2017). The subsequent closure of the Palaeo-Turkestan Ocean in the Late Carboniferous resulted in voluminous, ca. 300–285 Ma post-collisional, granitoid magmatism during the Early Permian (Biske & Seltmann, 2010; Dolgopolova et al., 2017; Konopelko, Seltmann, et al., 2017; Seltmann et al., 2011).

The Mesozoic history of the Tian Shan is dominated by deformation caused by the collision of Cimmerian continental fragments with the southern margin of Eurasia (e.g., De Grave et al., 2012; Käßner, Ratschbacher, Pfänder, et al., 2017). This period of Mesozoic deformation was initiated by the closure of the Palaeo-Asian Ocean at the end of the Permian to the earliest Triassic (e.g., Li et al., 2016; Xiao et al., 2009). Subduction of the Palaeo-Tethys beneath Eurasia initiated in the Triassic, leading to the collision of the Qiangtang block to the southern Eurasian margin, which is thought to have induced extensive deformation to the Tian Shan (e.g., De Grave et al., 2011; Glorie & De Grave 2016; Ratschbacher et al., 2003; Robinson, 2015). Subduction and accretion to the southern margin of Eurasia continued further south during the Jurassic and Early Cretaceous, culminating in the final closure of the Palaeo-Tethys Ocean (e.g., Kapp et al., 2007; Robinson, 2015). Rapid Late Jurassic-Cretaceous cooling has been documented for the Kyrgyz Tian Shan (to the east of the TFF; e.g., De Grave et al., 2013; Nachtergaele et al., 2018). In contrast, the extent of Jurassic and Cretaceous cooling in the westernmost Tian Shan (to the west of the TFF) is poorly defined. During the Late Jurassic-Early Cretaceous, coal deposits formed along the eastern margin of the Chatkal-Kurama terrane (Angren; Figure 2), suggesting a marine environment (Ahmedov, 2000; Dill et al., 2008). To the south, the Fergana Basin (Figure 1) is characterized by basal sections of Jurassic conglomerate fining upward into Jurassic and Cretaceous sedimentary sequences, indicating that the Fergana Basin experienced marine incursions of the Paratethyan Sea (Bande, Sobel, Mikolaichuk, & Torres, 2017; Burov & Molnar, 1998; De Pelsmaeker et al., 2018; Nachtergaele et al., 2018). Detailed analysis of the Late Cretaceous marine sediments suggested that the region was covered by a marine environment at least twice, once in the Turonian and again in the Maastrichtian (Ahmedov, 2000).

During the Cenozoic, the Tian Shan experienced renewed deformation, generating much of the high relief that can be found today. Many authors have identified a dominant Cenozoic cooling signal within the Tian Shan, which is thought to be related with the India-Eurasia collision and subsequent Pamir indentations with the Eurasian margin (e.g., Aitchison et al., 2007; De Grave et al., 2007; Molnar & Tapponnier, 1975; Sobel, Chen, et al., 2006). In the western Tian Shan, previous studies have identified initiation of exhumation at ca. 30–

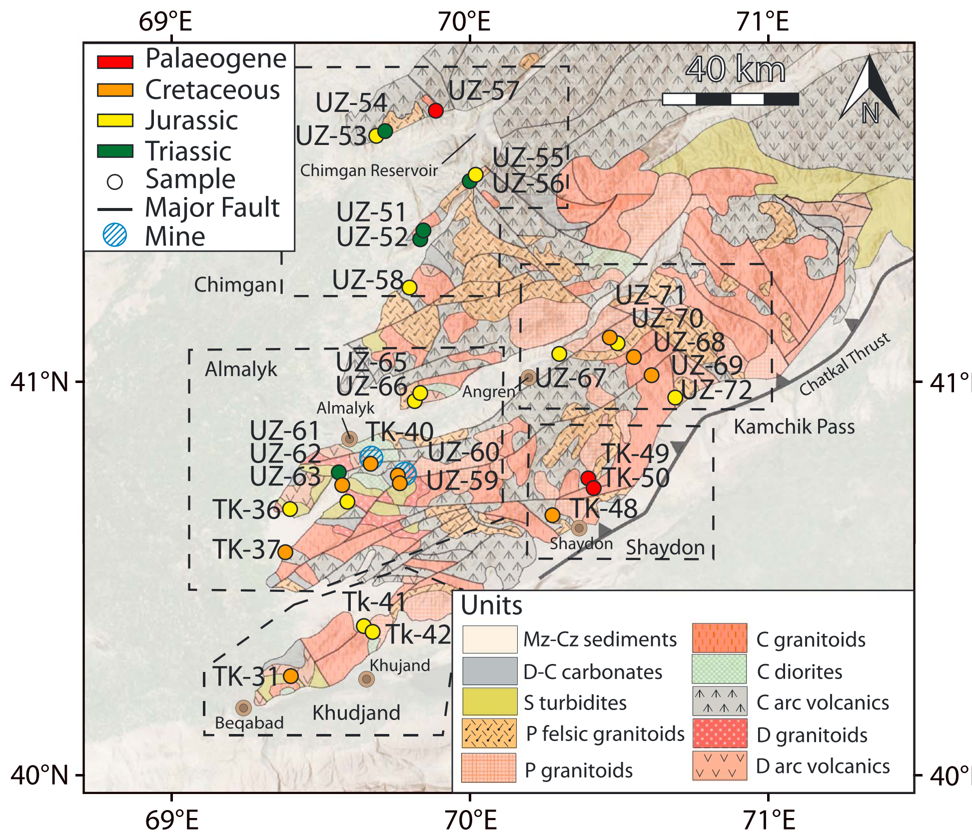

Figure 2. Geological map of the Chatkal-Kurama terrane modified from Dolgopolova et al. (2017). The map displays the locations for the apatite fission track (AFT) data obtained in this study. Sample symbols are color coded following AFT central ages. A detailed summary of the AFT data is available in supporting information S1. Mz is the Mesozoic, Cz is the Cenozoic, D is Devonian, C is the Carboniferous, S is the Silurian, and P is the Permian.

20 Ma and accelerating of exhumation since ca. 15–10 Ma, which correlates with periods of Pamir convergence (e.g., Bande, Sobel, Mikolaichuk, Schmidt, et al., 2017; Jepson et al., 2018; Käßner, Ratschbacher, Jonckheere, et al., 2017).

3. Methodology

New thermochronological data for 30 granitoid rock samples from the western Tian Shan are presented (Figure 2). Three different thermochronological methods were applied: (1) zircon (U-Th-Sm)/He dating (closure temperature of ~180 °C; Reiners et al., 2002); (2) apatite fission track thermochronology (partial annealing zone of ~120–60 °C; Wagner & Van den Haute, 1992); and (3) apatite (U-Th-Sm)/He dating (closure temperature of ~80–40 °C; Zeitler et al., 1987).

3.1. Apatite Fission Track Analysis

The apatite fission track method is based on the temperature-dependent annealing of mineral lattice damage features, known as *fission tracks*, that are created by the spontaneous decay of ^{238}U (Wagner & Van den Haute, 1992). Fission tracks record the thermal history of a rock sample through the apatite partial annealing zone (APAZ) of ~120–60 °C (Green, 1986). Apatite grains were picked and mounted in epoxy resin, then polished to expose internal sections, and were subsequently chemically etched in a 5-M HNO_3 solution for 20 s at 20 °C to reveal the natural spontaneous fission tracks. Fission track analysis was performed at The University of Adelaide using an Autoscan system. The concentration of uranium (^{238}U) and chlorine (^{35}Cl) of each apatite grain was measured using laser ablation-inductively coupled plasma-mass spectrometry. Data reduction was performed in Iolite using the Trace Elements DRS (Paton et al., 2011). Instrumental drift correction was carried out using Madagascar apatite as an external standard, and elemental concentrations were calculated using ^{43}Ca as the internal standard. Age calculation was carried out as described in Hasebe et al. (2004) and De Grave et al. (2012), using the Durango apatite (McDowell et al., 2005) to perform a ζ calibration (Vermeesch, 2017). Apatite fission track central ages were determined using RadialPlotter (Vermeesch, 2009), and individual radial plots can be found in supporting information S3. A duplicate sample was made for TK-50 and irradiated using californium (^{252}Cf) at The University of Melbourne in order to increase the likelihood of measuring a sufficient amount of confined tracks for thermal history reconstructions (Donelick & Miller, 1991). For a detailed methodology, see Glorie et al. (2017) and Gillespie et al. (2017).

3.2. Apatite and Zircon (U-Th-Sm)/He

The (U-Th-Sm)/He thermochronometers are based on the diffusivity of ^{4}He. The thermal sensitivity for apatite helium (AHe) is 80–40 °C, making it valuable for constraining the most recent thermal cooling event (Farley, 2002; Zeitler et al., 1987). For zircon, the thermochronometer records the thermal history at ~190–170 °C (Guenthner et al., 2013; Reiners et al., 2002). The (U-Th-Sm)/He analyses for this study were undertaken at the John de Laeter Centre, Curtin University, and followed the protocols described in Danišík et al. (2012).

Apatite and zircon crystals were hand-picked following the recommendations of Farley (2002), photographed and measured for physical dimensions, before being loaded in Pt (apatite) and Nb (zircon) microtubes. Helium (^{4}He) was extracted from apatite at ~900 °C, under ultra-high vacuum using a diode laser and measured by isotope dilution on a Pfeiffer Prisma QMS-200 mass spectrometer. A *re-extract* was run after each sample to verify complete outgassing of the crystals. Helium gas results were corrected for blank, determined by heating empty microtubes using the same procedure. After the ^{4}He measurements, tubes containing the crystals were retrieved from the laser cell, spiked with ^{235}U and ^{230}Th, and dissolved. Sample, blank, and spiked standard solutions were analyzed by isotope dilution for ^{238}U and ^{232}Th and by external calibration for ^{147}Sm on an Agilent 7500 inductively coupled plasma-mass spectrometry. The total analytical uncertainty was calculated as a square root of the sum of squares of uncertainty on He and weighted uncertainties on U, Th, Sm, and He measurements and is typically $<5\%$ (1σ). The raw (U-Th-Sm)/He ages were corrected for alpha ejection (F_T correction) after Farley et al. (1996), whereby a homogenous distribution of U, Th, and Sm was assumed for the crystals. Replicate analyses of internal standard Durango apatite (n = 10) measured over the period of this study yielded mean (U-Th-Sm)/He ages of 31.9 ± 1.9 Ma (1σ), consistent with the reference Durango (U-Th-Sm)/He age of 31.02 ± 1.01 Ma (McDowell et al., 2005). For the Fish Canyon zircon, we acquired 28.6 ± 0.8 Ma (n = 10), which is in excellent agreement with the reference age of Reiners (2005) at 28.3 ± 1.3 Ma.

3.3. Thermal History Modeling

Thermal history modeling was performed on a total of 24 samples, with a sufficient number of confined tracks ($>$10, although less tracks indicates less precision). The QTQt software (version 5.5.0) was applied, which uses Bayesian transdimensional Markov Chain Monte Carlo statistics to determine models for the cooling pathway of the sample (Gallagher, 2012). Along with the confined track length, individual Apatite Fission Track Analysis (AFT), AHe, and ZHe ages were used in the modeling procedure. The concentration of ^{35}Cl was used as a kinetic parameter (Donelick et al., 2005). More details on the modeling approach can be found in Gallagher (2012) and Gillespie et al., (2017).

4. Results

For a systematic and thorough discussion, the results for the 30 samples in this study will be subdivided into five groups based on regional proximity to each other (Figure 2). The groups are named after nearby towns or mountain passes and will be discussed from north to south and are as follows: (1) Chimgan, (2) Kamchik Pass, (3) Almalyk, (4) Shaydon, and (5) Khudjand (Figure 2). Tables 1 and 2 summarize the AFT and (U-Th-Sm)/He data. Detailed tables and figures for all single grain AFT, (U-Th-Sm)/He, mean track length (MTL) data, and individual thermal history models are available in supporting information S1–S6.

4.1. Chimgan Region

Eight granitoid samples were collected in the southern Chatkal Mountains surrounding Chimgan reservoir, in the north of our study area (Figure 2). The majority of samples from the Chimgan region display a Triassic AFT central age. Samples UZ-52, UZ-54, and UZ-56 yield unimodal AFT ages of 235 ± 20, 207 ± 4, and 219 ± 6 Ma,

Table 1
Apatite Fission Track Data

Sample	Latitude	Longitude	Elevation (m)	*n*	Age (Ma)	±1σ (Ma)	No. of lengths	Lengths (μm)	±1σ (μm)
Chimgan									
UZ-51	41.391	69.857	1,919	32	225.0	6.8	65	12.4	1.2
UZ-52	41.395	69.861	1,769	5	235.0	20.0	—	—	—
UZ-53	41.629	69.725	1,524	38	154.2	5.5	115	12.1	1.5
UZ-54	41.628	69.724	1,109	37	207.2	4.4	170	12.4	1.1
UZ-55	41.528	70.024	1,396	33	174.0	10.0	34	12.0	1.7
UZ-56	41.517	70.014	1,909	34	218.9	6.3	64	12.7	1.3
UZ-57	41.684	69.894	1,438	22	28.5	3.7	45	12.7	1.5
UZ-58	41.245	69.808	1,207	31	171.3	7.5	31	12.7	1.6
Kamchick Pass									
UZ-67	41.072	70.271	1,136	37	199.6	8.4	18	12.0	1.5
UZ-68	41.073	70.558	2,139	27	135.0	12.0	24	11.8	1.1
UZ-69	41.027	70.609	1,688	19	94.4	6.1	18	11.2	1.7
UZ-70	41.110	70.505	2,061	27	156.0	15.0	13	11.4	1.2
UZ-71	41.125	70.479	1,620	31	96.8	5.0	36	12.1	1.8
UZ-72	40.997	70.789	1,530	41	167.0	12.0	63	12.1	1.4
Almalyk									
UZ-59	40.775	69.778	1,041	31	100.0	9.1	27	11.7	1.6
UZ-60	40.768	69.781	1,222	39	141.4	8.4	51	12.4	1.3
UZ-61	40.772	69.586	705	38	205.8	6.4	34	12.9	1.0
UZ-62	40.752	69.591	752	28	143.8	8.6	66	13.0	1.2
UZ-63	40.712	69.603	878	39	182.0	9.8	56	12.8	1.2
UZ-65	40.950	69.824	827	17	187.0	14.0	17	12.4	1.0
UZ-66	40.971	69.838	915	31	196.0	12.0	61	12.9	1.0
TK-36	40.674	69.401	540	28	183.0	11.0	63	13.1	0.9
TK-37	40.576	69.396	489	35	103.6	5.1	14	12.0	2.2
TK-40	40.799	69.690	864	14	116.1	5.5	—	—	—
Shaydon									
TK-48	40.678	70.292	1,024	22	124.0	12.0	—	—	—
TK-49	40.746	70.426	1,192	10	32.0	10.0	—	—	—
TK-50	40.768	70.410	1,304	33	31.4	3.4	20	12.7	0.8
Khudjand									
TK-31	40.254	69.408	500	40	131.0	5.0	75	11.9	1.5
TK-41	40.397	69.660	633	34	163.9	4.8	99	13.3	1.1
TK-42	40.379	69.683	540	20	176.0	10.0	—	—	—

Note. n is the number of grains analyzed per sample, and no. of lengths is the number of confined track lengths identified in each sample.

respectively (Table 1). Samples UZ-54 and UZ-56 produced MTLs of 12.4 ± 1.1 and 12.7 ± 1.3 μm. Sample UZ-51 displays a slightly bimodal age distribution, with 80% of the single grain ages preserving a similar Triassic age (225 ± 7 Ma) and 20% of single grain ages recording a Palaeogene signal (ca. 52 ± 5 Ma; supporting information S3). Samples UZ-53, UZ-55, and UZ-58, which were sampled at slightly lower elevations (Table 1), yield ages of 155 ± 6, 174 ± 10, and 171 ± 8 Ma. Furthermore, they display reduced MTL values and broader confined track length distributions compared to the Triassic samples (Table 1 and supporting information S4). The most northerly sample (UZ-57), which was sampled in the Chatkal Ranges (an area of slightly higher relief; ~2,000 m, Figure 1), gave a younger AFT central age of 29 ± 4 Ma, with a MTL of 12.7 ± 1.5 μm (Table 1 and supporting information S4).

4.2. Kamchik Pass Transect

A series of samples were taken over an elevation profile across Kamchik Pass across the eastern limb of the Chatkal-Kurama terrane (Figure 2). In total, six granitoid samples were taken with a minimum of ~150 m vertical distance between neighboring samples and were grouped into the Kamchik Pass transect.

The AFT central ages from the Kamchik Pass samples can be separated into Jurassic and Cretaceous ages. Sample UZ-67, east of the main sample transect, produced an AFT central age of 200 ± 8 Ma and a MTL of 12.0 ± 1.5 μm. Samples UZ-70 and UZ-72 were taken at low elevations along the Kamchik pass transect and yielded Jurassic central ages of 156 ± 15 and 167 ± 12 Ma (Figure 2). The MTL for the sample that

Table 2
Mean Zircon (U-Th-Sm)/He and Apatite (U-Th-Sm)/He Age and Chemistry Data

Sample	^{232}Th (ng)	± (%)	^{238}U (ng)	± (%)	^{147}Sm (ng)	± (%)	He (ncc)	± (%)	Total analytical uncertainty (%)	Th/U	Raw age (Ma)	±1σ (Ma)	Ft	Cor. age (Ma)	±1σ (Ma)
Zircon (U-Th-Sm)/He data															
TK-42	1.132	1.4	2.683	1.9	0.002	18.2	53.137	1.0	2.039	0.5	159.5	3.2	0.70	229.0	6.2
TK-36	1.077	1.4	4.027	1.9	0.002	14.9	93.629	0.7	1.952	0.3	179.9	3.5	0.72	244.4	8.1
Apatite (U-Th-Sm)/He data															
UZ-69	0.111	3.8	0.051	4.0	0.022	0.3	0.075	2.4	3.818	2.2	8.0	0.3	0.60	13.5	1.3
TK-50	0.119	3.9	0.067	4.1	0.041	0.2	0.175	2.2	4.045	1.8	12.7	0.5	0.69	18.2	1.2
TK-49	0.056	4.1	0.039	4.2	0.011	0.4	0.130	2.1	4.032	1.4	20.8	0.8	0.53	27.5	2.5
TK-41	0.143	5.2	0.067	5.3	0.021	0.4	1.011	2.6	4.888	2.3	69.1	3.5	0.65	125.8	6.3
TK-36	0.097	4.7	0.093	4.9	0.014	0.4	1.513	2.7	4.911	1.0	110.5	5.3	0.71	178.6	8.9

Note. For single grain analysis, see Table S2. Concentrations of thorium, uranium, and samarium in ng, He is the concentration of helium measured in ncc, and Th/U is the ratio of thorium to uranium. Raw age is the age before the F_T correction is made. F_T is the alpha-ejection correction parameter of Farley et al. (1996). Cor. age is the age after applying the F_T correction, and TAU is the total analytical uncertainty.

produced a Middle Jurassic AFT age (UZ-72) is slightly longer compared to the Late Jurassic AFT sample (UZ-70; Table 1 and supporting information S4). Samples UZ-68, UZ-69, and UZ-71 yielded Cretaceous AFT ages of 135 ± 12, 94 ± 6, and 97 ± 5 Ma, respectively (Table 1 and Figure 2). The three Cretaceous AFT age samples yielded, on average, shorter MTLs compared to the Jurassic AFT samples (Table 1 and supporting information S4). The samples along Kamchik Pass show no clear age-elevation relationship. Based on apatite quality, sample UZ-69 was selected for AHe analysis and yielded a Cenozoic AHe age of 13.5 ± 1.3 Ma, which is significantly younger than the AFT ages obtained for Kamchik Pass (Table 2 and supporting information S2).

4.3. Almalyk Region

Ten samples were taken from mineral deposit hosting regions surrounding the town of Almalyk (Figure 2). This includes two samples taken in close vicinity to the Sari-Cheku porphyry copper-gold deposit (UZ-59 and UZ-60) and one sample from just south of the Kalmakyr porphyry deposit (TK-40; Seltmann & Porter, 2005).

The AFT central ages obtained for the 10 samples produced one Late Triassic age, four Jurassic ages, and five Cretaceous ages. A Late Triassic AFT age was obtained for sample UZ-61 of 206 ± 6 Ma. The four Jurassic AFT ages are recorded by UZ-63, UZ-65, UZ-66, and TK-36, displaying ages of 182 ± 10, 187 ± 14, 196 ± 13, and 183 ± 11 Ma, respectively. The three samples that were taken near mineral deposits yielded Late Cretaceous ages. Samples TK-40, UZ-59, and UZ-60 gave AFT ages of 116 ± 6, 100 ± 9, and 141 ± 8 Ma, respectively. Away from the deposits, Cretaceous AFT ages were recorded for samples TK-37 and UZ-62, with central ages of 104 ± 5 and 144 ± 9 Ma, respectively (Table 1 and Figure 2). Based on apatite and zircon quality, two samples were selected for AHe analysis, and one sample was selected for ZHe analysis. Sample TK-40 produced an AHe age of 143 ± 7 Ma, which is slightly older than its AFT age of 116 ± 6 Ma. The AHe age for TK-36, calculated as 179 ± 9 Ma, is within error to its AFT age of 183 ± 11 Ma. Sample TK-36 was also selected for ZHe analysis that yielded an age of 244 ± 8 Ma (Table 2). The Late Triassic-Early Jurassic samples of TK-36, UZ-61, UZ-63, UZ-65, and UZ-66 yielded, on average, longer MTLs when compared to the slightly shorter MTLs obtained by the Cretaceous samples UZ-59, UZ-60, and UZ-62 (Table 1 and supporting information S4).

4.4. Shaydon Region

The Shaydon region consists of three samples that were taken near the village of Shaydon, Tajikistan (Figure 2). Sample TK-48 yielded a Cretaceous central age of 124 ± 12 Ma. Samples TK-49 and TK-50 both yielded consistent Palaeogene AFT ages of 32 ± 10 and 31 ± 3 Ma, respectively (Table 1). AHe analysis was performed on both Palaeogene AFT age samples. For sample TK-49, an Oligocene AHe age of 28 ± 3 Ma was obtained that is within error to its AFT age, and for sample TK-50, a Miocene AHe age of 18 ± 1 Ma was obtained, which is slightly younger than its corresponding AFT age (Table 2). Sample TK-50 was selected for ^{252}Cf irradiation to obtain a sufficient quantity of confined tracks, producing a MTL of 12.7 ± 0.8 μm (Table 1).

4.5. Khudjand Region

The Khudjand region represents the most southwestern extent of the Chatkal-Kurama terrane, from which three samples were taken (TK-41, TK-42, and TK-31). Samples TK-41 and TK-42 both yielded Jurassic AFT central ages of 164 ± 5 and 176 ± 10 Ma, respectively. For sample TK-41, a MTL of 13.3 ± 1.1 μm was obtained. In contrast, sample TK-31 generated a Cretaceous AFT age of 131 ± 5 Ma and a shorter MTL of 11.9 ± 1.5 μm (Table 1). Based on apatite quality, sample TK-41 was selected for AHe analysis, producing a Cretaceous age of 126 ± 14 Ma that is slightly younger than its corresponding AFT age of 164 ± 5 Ma. Sample TK-42 was selected for ZHe analysis, yielding a Triassic age of 229 ± 6 Ma (Table 2).

4.6. Thermal History Models

Thermal history models were produced for samples with a sufficient quantity of confined tracks (>10; Table 1 and supporting information S5). Of the 30 samples analyzed in this study, 24 were suitable for thermal history modeling. Figure 3 displays all time-temperature models

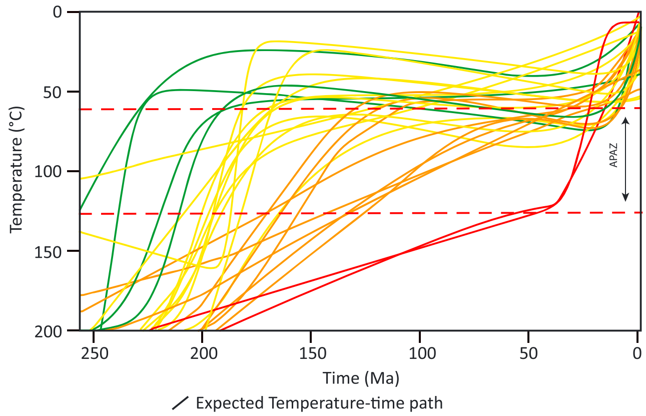

Figure 3. A plot displaying the modeled temperature-time paths for all samples within the Chatkal-Kurama terrane that yielded sufficient confined track data for modeling purposes. Modeling was performed using QTQt Gallagher (2012). Where available, apatite and zircon (U-Th-Sm)/He data were incorporated into its respective thermal history model. The temperature-time path is colored according to apatite fission track central age; green is Triassic, yellow is Jurassic, orange is cretaceous, and red is Palaeogene. The red dashed line represents the apatite partial annealing zone (APAZ). This figure demonstrates the relationship between Cretaceous apatite fission track age and increased residence time in the APAZ. Individual sample histograms and temperature-time plots are available in supporting information S4 and S5, and the used criteria for thermal modeling are tabulated in supporting information S6.

calculated for the Chatkal-Kurama terrane. Detailed individual thermal models for each sample and modeling parameters are available in supporting information S5 and S6 (Flowers et al., 2015).

The thermal history models in this study show a distinct relationship between samples with a similar AFT age and the rate of cooling for the thermal pathway obtained. The Triassic AFT age samples UZ-51, UZ-54, and UZ-56 from the Chimgan region and sample UZ-61 from the Almalyk region (green models in Figure 3) display rapid cooling through the APAZ during the Triassic (ca. 250–220 Ma) followed by a long period of thermal stability during most of the Mesozoic and Cenozoic. The Triassic-aged thermal history models for samples UZ-51 and UZ-54 show a return to the APAZ before a subsequent cooling pulse since ca. 25 Ma; however, this is not well pronounced (Figure 3). The thermal history models for the Early Jurassic AFT age samples TK-36, UZ-63, UZ-65, and UZ-66 from the Almlyk region and sample TK-41 from the Khudjand region (yellow models in Figure 3) show cooling through the APAZ during the latest Triassic-Early Jurassic (ca. 215–190 Ma). The Jurassic AFT samples display a similar thermal history to the models obtained for the Triassic AFT age samples, relatively fast cooling in the Early Jurassic, followed by thermal quiescence (or slight reheating) during most of the Late Jurassic-Palaeogene. Several samples were affected by renewed cooling since ca. 35 Ma. The Late Jurassic AFT samples UZ-53, UZ-55, and UZ-58 from the Chimgan region and samples UZ-67, UZ-70, and UZ-72 from the Kamchik Pass all display very similar thermal history models to those obtained for the Lower Jurassic AFT samples. However, the initial cooling during the Jurassic through the APAZ was slower. The Cretaceous AFT age samples UZ-69, UZ-69, and UZ-71 from the Kamchik Pass, samples UZ-59, UZ-60, and UZ-62 from the Almalyk region, and sample TK-31 from the Khudjand region (orange models in Figure 3) display rather slow cooling and increased residence time in the APAZ during the Cretaceous, followed by a renewed onset of cooling since ca. 30 Ma. Finally, the two Cenozoic samples, UZ-57 from the Chimgan region and TK-50 from the Shaydon region (red models in Figure 3), both display fast cooling through the APAZ since ca. 35 Ma (Figure 3 and supporting information S5). In summary, the thermal history models indicate rapid cooling during the Triassic-Early Jurassic (ca. 250–190 Ma), slow cooling or thermal quiescence during the Late Jurassic-Palaeogene, and renewed cooling during the Neogene (ca. 35-25 Ma).

5. Interpretation and Discussion

5.1. Thermochronological Interpretations

The sample locations within the Chatkal-Kurama terrane range from the southwestern margin of the terrane, near Khudjand, to the Uzbekistan-Kazakhstan border around the Chimgan reservoir in the north (Figure 2). Over this geographic extent, the obtained AFT ages display a clear younging trend from the northwest to the southeast. The oldest (Triassic) AFT ages from the Chatkal-Kurama terrane were obtained on the northwestern margin. Toward the southeast, a mixture of Jurassic and Cretaceous AFT ages were obtained, with Cretaceous ages becoming more abundant further south and near the mineral deposits in the Almalyk region. The youngest AFT ages identified in this study were obtained in the north of the study area (in the Chatkal Ranges) and in the southeast of the Chatkal-Kurama terrane, at the margin of the Fergana Basin (Figure 2).

As illustrated by the thermal history models (Figure 3), the Triassic and Early Jurassic AFT age samples cooled rapidly to the surface at that time and remained unaffected by any later thermal activity. The mid to Late Jurassic and Cretaceous AFT age samples underwent more protracted residence in the APAZ and partially record the subsequent Cenozoic cooling identified in the Cenozoic AFT age samples. This pattern can be illustrated by plotting the MTL values for each sample against their corresponding AFT central ages (Figure 4). In this plot, our new data from the Chatkal-Kurama terrane is combined with Bande, Sobel, Mikolaichuk, and

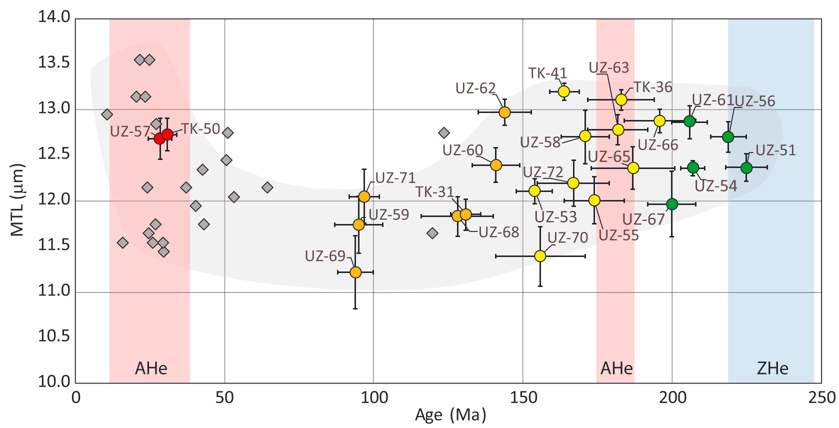

Figure 4. A *boomerang* plot displaying apatite fission track (AFT) central age against mean track lengths (MTLs). Circles denote AFT data obtained in this study, and diamond symbols are data from Bande, Sobel, Mikolaichuk, and Torres, (2017). Color coding is the same as in previous figures and represents central AFT ages; green is Triassic, yellow is Jurassic, orange is Cretaceous, and red is Palaeogene. The x axis error bars are the $\pm 1\sigma$ standard deviations, and the vertical error bars are standard errors of the mean. The red and blue shaded bars represent the age and $\pm 1\sigma$ uncertainties for the apatite helium (AHe) and zircon helium (ZHe) data obtained in this study, respectively. This plot highlights a period of fast cooling in the Triassic-Early Jurassic, followed by slow cooling in the Late Jurassic-Cretaceous, before showing a return to fast cooling in the Cenozoic.

Torres (2017) from the adjoining Chatkal Ranges in western Kyrgyzstan and display a characteristic *boomerang* trend (Gallagher, 2012; Green et al., 1986). The longer MTLs suggest faster cooling, while shorter MTLs reflect prolonged residence in the APAZ. The *boomerang plot* demonstrates that the Triassic and Early Jurassic AFT ages are indicative of a significant thermal event at that time. The Late Jurassic and Cretaceous AFT ages correspond to shorter MTLs and are thus slowly cooled APAZ residence ages. In the Late Palaeogene, the boomerang begins to curve back up toward longer MTLs, suggesting the start of a second thermal event (Figure 4). The latter event is better exposed in the higher relief of the Chatkal Ranges (Figure 1; Bande, Sobel, Mikolaichuk, & Torres, 2017), but also the southeastern margin on the Chatkal-Kurama terrane, along the Fergana basin margin.

The (U-Th-Sm)/He data obtained in this study further illustrate the two thermal events that were identified in the boomerang plot and thermal history models (during the Triassic and Late Palaeogene-Early Neogene; Figures 3 and 4). The ZHe ages (ca. 250–225 Ma, TK-42 and TK-36) are in agreement with the Triassic AFT ages obtained from sample TK-42. Additionally, sample TK-36 yielded an Early Jurassic AHe age (ca. 180 Ma) that is within error to its corresponding AFT age (183 ± 11 Ma; Table 2 and Figure 4). These results strengthen the claim that the Chatkal-Kurama terrane underwent fast cooling during the Triassic-Early Jurassic. Samples TK-41 and TK-40 yielded scattered Late Jurassic-Cretaceous AHe ages that were significantly younger or older than their corresponding AFT age (163 ± 5 Ma), suggesting slow cooling at that time (Table 2 and supporting information S2). Late Palaeogene-Early Neogene AHe ages (ca. 28–14 Ma, UZ-69, TK-49, and TK-50) chronologically match corresponding AFT ages (ca. 31 Ma), suggesting renewed cooling began during the Palaeogene, as illustrated by the thermal history models and boomerang plot (Figures 3 and 4 and Table 2).

The significant geographic younging trend throughout the Chatkal-Kurama terrane reflects the progressive influence of a Cenozoic thermal pulse from northwest to southeast. The northwestern section of the Chatkal-Kurama terrane (excluding the Cenozoic AFT sample in the Chatkal Ranges) effectively represents a Triassic-Early Jurassic palaeo-surface while the Chatkal-Kurama terrane was, in our interpretation, progressively exhumed toward the southeast, during the Cenozoic. In addition, we suggest that the progressive exhumation to the southeast reflects a process of fault-block tilting. This Cenozoic tilting process exposed a deeper section of the thermal history of the Chatkal-Kurama terrane (that was at lower APAZ temperatures during the Cretaceous) in the southeast with respect to the northwest.

The Chatkal-Kurama terrane is bounded to the northwest by the Syrdarya Block, which represents a Mesoproterozoic to Neoproterozoic continental block, a part of the Kazakhstan palaeocontinent (Dolgopolova et al., 2017; Konopelko, Klemd, et al., 2017; Samygin & Burtman, 2009). To the southeast of the Chatkal-Kurama terrane, the Fergana Basin basement is a rigid piece of Paleozoic crust (Figure 2; Burov & Molnar, 1998). Both the Syrdarya Block and the Fergana basement are strong units within the Central Asian edifice that transmit stress from distant collisions at the Eurasian plate margins. The Chatkal-Kurama terrane is composed of weaker crust (e.g., volcanic arc) that is more easily deformed than the surrounding rigid block of the Fergana and Syrdarya blocks. Therefore, the crustal tilting can be explained by different crustal strengths in response to distant stresses. The northeast of the Chatkal-Kurama terrane was held in place along the margin of the Syrdarya Block, leading to the preservation of Triassic cooling ages, while the continental collisions on the southern Eurasian margin drove progressive tilting of the Chatkal-Kurama terrane, toward the Fergana basin margin, as demonstrated by the Cretaceous and Palaeogene AFT and AHe ages (Figure 1).

5.2. Thermotectonic Evolution of the Chatkal-Kurama Terrane

5.2.1. Triassic-Early Jurassic

This study reports a Triassic-Early Jurassic fast cooling pulse experienced by the Chatkal-Kurama terrane (Figures 2, 3, and 4 and Table 2). The oldest thermochronological ages obtained from the northwestern margin of the Chatkal-Kurama terrane are the Triassic ZHe (245 and 229 Ma) and AFT ages (225 Ma) from samples TK-36, TK-42, and UZ-51 (Figure 4). In comparison, the youngest age of magmatism identified in the Chatkal-Kurama terrane is Permian (ca. 286 Ma; Konopelko, Seltmann, et al., 2017). Therefore, a direct thermal relationship between the Triassic AFT ages to postmagmatic cooling can be excluded.

Previous thermochronological studies in the Tian Shan ascribe Triassic-Early Jurassic AFT ages to the closure of the Palaeo-Asian Ocean in the Permian and the subsequent collision of the Qiangtang Block with the Eurasian margin (e.g., De Grave et al., 2011; Glorie et al., 2010; Glorie & De Grave 2016; Macaulay et al., 2014; Xiao et al., 2009). During this period, samples along the northwestern margin of the Chatkal-Kurama terrane were rapidly cooled to surface temperatures. Thus, we interpret the Triassic-Early Jurassic fast cooling signal in our data to be related with the exhumation associated with the closure of the Palaeo-Asian Ocean and/or the Qiangtang convergence in the Triassic-Early Jurassic.

5.2.2. Late Jurassic-Cretaceous

In the Chatkal-Kurama terrane, our data are indicative of protracted residence in the APAZ during the Late Jurassic-Early Cretaceous, suggesting that the Chatkal-Kurama terrane experienced a period of steady, slow denudation and tectonic quiescence at that time (Figure 3). In the Late Jurassic-Cretaceous, thermotectonic quiescence induced planation and punctuated marine incursions of the Paratethyan Sea (Bande, Radjabov, et al., 2017; Burov & Molnar, 1998; Carrapa et al., 2015; De Pelsmaeker et al., 2018; Nachtergaele et al., 2018). These marine incursions deposited thick Jurassic and Cretaceous sedimentary sequences, conglomerates, and coal deposits (Ahmedov, 2000; Dill et al., 2008).

5.2.3. Cenozoic

The presence of a Cenozoic fast cooling signal for the Chatkal-Kurama terrane (both in this study and Bande, Sobel, Mikolaichuk, and Torres, 2017) is evident by overlapping ages for multiple thermochronometers (AFT and AHe), in combination with long MTLs and associated thermal history models (Figures 3 and 4). Bande, Sobel, Mikolaichuk, and Torres (2017) interpret this thermal event to deformation in the Chatkal-Kurama caused by the Cenozoic reactivation of the Talas-Fergana Fault (Sobel & Dumitru, 1997). Similarly, the Cenozoic thermochronological ages identified in the southeastern margin are likely in response to stresses from the reactivation of the Talas-Fergana Fault transmitting both along the TFF and the Fergana Basin into the Chatkal-Kurama terrane. The appearance of Palaeogene fast cooling stands in contrast to the tectonic hiatus during the Late Jurassic to Miocene suggested by other thermochronological studies in the region (e.g., Käßner, Ratschbacher, Jonckheere, et al., 2017). The Palaeogene sample in the northeastern part of the Chatkal-Kurama Range (UZ-57) displays a similar thermal history to samples identified by Bande, Sobel, Mikolaichuk, and Torres (2017), suggesting that this sample has been exhumed, likely in response to the deformation along the TFF, rather than preserving a Triassic-Jurassic AFT age, documented by samples taken from the northwestern margin with the Syr Darya Basin (UZ-53 and UZ-54; Figure 2). In the southwest of the Chatkal-Kurama, two samples with Palaeogene AFT ages (TK-49 and TK-50) occur along the Chatkal Thrust (Figure 2), along strike to Palaeogene AFT aged samples recorded by Bande, Sobel, Mikolaichuk, and Torres, 2017 (Figure 1). This suggests that the deformation caused by the India-Eurasia collision in the Palaeogene must have affected the Eurasian interior, causing fault reactivation and block-rotation of the Chatkal-Kurama terrane driven by the Chatkal Thrust and the TFF (Figure 2; Burov & Molnar, 1998; Bande, Sobel, Mikolaichuk, & Torres, 2017), exposing and cooling samples collected along the southern margin of this terrane through the APAZ. In addition, the Cenozoic reactivation of the Chatkal-Kurama terrane likely provided a source for the thick Cenozoic sedimentary sequences identified in the nearby Fergana Basin (Ahmedov, 2000; Bande, Sobel, Mikolaichuk, & Torres, 2017; De Pelsmaeker et al., 2018).

5.2.4. Regional Trends for the Western Tian Shan

The following section aims to integrate the thermochronological results obtained for the Chatkal-Kurama into the greater western Tian Shan thermotectonic history. In this study, we define the western Tian Shan as the section of the Tian Shan within the former Soviet Republics (Tajikistan, Uzbekistan, Kyrgyzstan, and Kazakhstan). The Mesozoic and Cenozoic thermotectonic evolution of the Chatkal-Kurama terrane is comparable to previous studies within the western Tian Shan (e.g., De Grave et al., 2013; Glorie et al., 2011; Käßner, Ratschbacher, Pfänder, et al., 2017; Sobel, Chen, et al., 2006), demonstrating that the western Tian Shan underwent a cyclical tectonic evolution of deformation, quiescence, and reactivation as a result of strain propagation from the Eurasian margin into the Central Asian interior.

The relationship between the tectonic history of the Chatkal-Kurama terrane and the western Tian Shan is demonstrated in Figure 5. Figure 5a represents a boomerang plot for all AFT age and length data obtained in the western Tian Shan (latitudinal and longitudinal constraints were placed at 40.000°N and 77.140°E, respectively), allowing for a direct comparison between the AFT age and length data of the Chatkal-Kurama terrane (west of the TFF) and Kyrgyz western Tian Shan (east of the TFF). The plot shows that both the Chatkal-Kurama terrane and the western Kyrgyz Tian Shan experienced a phase of fast cooling in the Triassic-Early Jurassic. However, while the Chatkal-Kurama terrane experienced a period of tectonic stability during the Late Jurassic-Cretaceous (low MTL values), the Kyrgyz western Tian Shan records prolonged fast cooling at that time (higher MTL values). From the Late Eocene-Early Oligocene, the western Tian Shan experienced the onset of renewed cooling as demonstrated by the increase in MTL values from corresponding Cenozoic AFT ages (Figure 5a).

The contrasting Mesozoic cooling histories on either side of the TFF are further explored in Figure 5b, which shows the geographical distribution of MTLs for the Mesozoic samples used in Figure 5a. The abundance of longer MTLs to the east of the TFF indicates that during the Mesozoic, areas to the east of the Talas-Fergana fault experienced more rapid exhumation compared to the west (Figure 5b). Particularly in close vicinity to the TFF, new AFT results from the Kyrgyz Tian Shan are indicative of Late Jurassic-Early Cretaceous basement cooling and denudation at that time (Nachtergaele et al., 2018). To the west of the TFF, MTL values are lower, suggesting slow cooling and flattening of the preexisting Mesozoic relief. Bande, Sobel, Mikolaichuk, and Torres (2017) and De Pelsmaeker et al. (2018) suggest that during the Cretaceous, much of the Chatkal-Kurama terrane was submerged by a marine incursion of the Paratethys Sea, while the North Tian Shan remained tectonically active. In this model, the Talas-Fergana Fault partitions strain from the Eurasian margin into the area to the east of the fault, causing deformation, while leaving the Chatkal-Kurama terrane relatively undeformed. De Pelsmaeker et al. (2018) proposed a model for the paleogeography of the western Tian Shan during the Late Jurassic-Early Cretaceous. The AFT data obtained in this study fit very well with this model and strengthen the hypothesis that the TFF acted as a topographic divide between the high eastern and low western Tian Shan during the Cretaceous. Figure 5b shows a slight modification to the model proposed by De Pelsmaeker et al. (2018); by incorporating published AFT data from the western Tian Shan we show that the marine transition zone occurred much closer to the major regional faults, to accommodate for the shorter MTLs near the northern margin of the Kyrgyz Tian Shan (Suusamyr valley; Glorie et al., 2010) and near the Kyrgyz Chatkal Ranges southeastern piedmonts (Bande, Sobel, Mikolaichuk, & Torres, 2017). As shown, the regions that record relatively short MTLs were covered by the marine incursion of the Paratethys or are located within a transitional zone during the Late Jurassic-Early Cretaceous, while high relief maintained to the east of the TFF (Figure 5b).

Given the widespread occurrence of Late Jurassic conglomerate deposits in the Tarim and Junggar basins, the fast, Late Jurassic cooling signal in the Kyrgyz Tian Shan is attributed to exhumation and denudation (Figure 5a; Dumitru et al., 2001; Glorie & De Grave 2016; Jolivet et al., 2013). The contrast between slow cooling, tectonic stability in the Chatkal-Kurama terrane and fast cooling, tectonic activity in the Kyrgyz western Tian Shan (west of the TFF) continues through to the end of the Early Cretaceous. During the Late Cretaceous and early Palaeogene, the entire western Tian Shan records slow cooling or tectonic quiescence, leading to the development of widespread planation surfaces (e.g., Bazhenov et al., 1993; Burbank et al., 1999; Glorie et al., 2010; Jolivet et al., 2013).

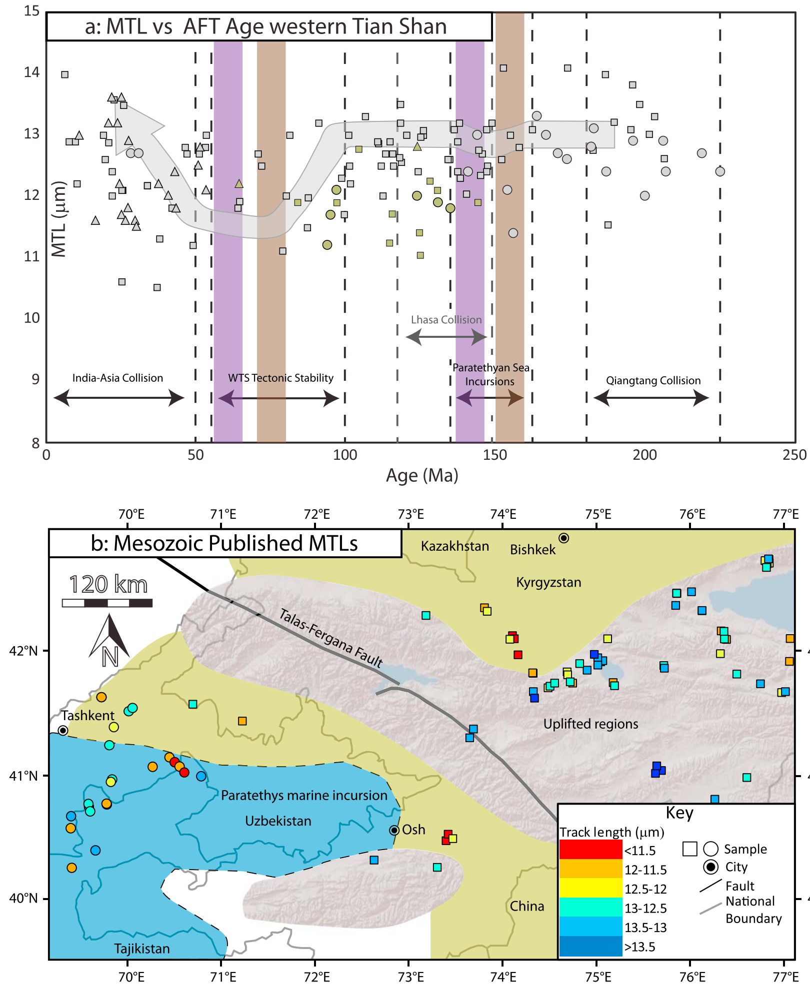

Figure 5. (a) A boomerang plot displaying apatite fission track central age against mean track length (MTL) for the western Tian Shan. Circle symbols identify the samples obtained in this study, the triangles are from samples in Bande, Sobel, Mikolaichuk, and Torres (2017), and the squares represent data obtained from other published apatite fission track (AFT) data in the Tian Shan (Bande, Radjabov, et al., 2017; Bande, Sobel, Mikolaichuk, Schmidt, et al., 2017; De Grave et al., 2011, 2012, 2013; Glorie et al., 2010, 2011; Käßner, Ratschbacher, Jonckheere, et al., 2017; Nachtergaele et al., 2018; Sobel, Chen, et al., 2006; Thiede et al., 2013). The color code of the symbols denotes the sample locations in Figure 5b. Green colored coded symbols identify samples that were assessed to lie in marine-mountain transition zone, and gray color coded symbols identify samples that lie in the mountainous zone. The brown shaded bars represent periods of conglomerate formation experienced in the Tian Shan, the purple shaded bars represent periods of planation identified the Tian Shan, and the dashed lines represent major tectonic events that impacted the Mesozoic western Tian Shan. (b) A map of the western extent of the Tian Shan displaying the MTL of published Mesozoic AFT data for the region, modified from De Pelsmaeker et al. (2018). The higher abundance of MTLs to the east of the Talas-Fergana Fault (TFF) is an indication that the Kyrgyz Tian Shan experienced a longer period of deformation and exhumation during the Mesozoic, when compared to the Chatkal-Kurama terrane to the west of the TFF. Blue regions represent areas of marine incursion during the Mesozoic, green regions represent areas of marine-mountain transition, and the gray regions represent areas that were uplifted in the Mesozoic (after De Pelsmaeker et al., 2018). Circles represent data obtained by this study. Published AFT data are represented by squares, obtained from Glorie et al. (2010, 2011), De Grave et al. (2011, 2012, 2013), Macaulay et al. (2014), and De Pelsmaeker et al. (2018).

The collision of India with Eurasia and the subsequent Pamir indentation during the Cenozoic marked the end of this period of tectonic stability (e.g., Kapp et al., 2007; Schwab et al., 2004). The stress from these Cenozoic collisions partitioned strain into the continental interior of Eurasia via major faults (Glorie et al., 2010; Sobel, Chen, et al., 2006). These collisions continued to be the dominant control on the reactivation and exhumation that has been identified throughout the Tian Shan and the Chatkal-Kurama terrane in the Cenozoic (Figure 5a; e.g., Bande, Sobel, Mikolaichuk, & Torres, 2017; Käßner, Ratschbacher, Jonckheere, et al., 2017; Bande, Sobel, Mikolaichuk, Schmidt, et al., 2017; De Grave et al., 2012; Macaulay et al., 2014). Within our study area, fast Cenozoic cooling was revealed for the southeastern margin of the Chatkal-Kurama terrane (samples TK-49, TK-50, and UZ-69), which were induced by crustal tilting and fault reactivation. This observation is in good agreement with other studies that describe reactivation and deformation since ca. 30–20 Ma, with a significant increase across the Tian Shan in the last ca. 10 Ma (Bande, Sobel, Mikolaichuk, Schmidt, et al, 2017; De Grave et al., 2011, 2013; Glorie et al., 2010, 2011; Jepson et al., 2018; Käßner, Ratschbacher, Jonckheere, et al., 2017; Macaulay et al., 2014; Sobel & Dumitru, 1997; Sobel, Chen, et al., 2006; Sobel, Oskin, et al., 2006).

6. Conclusion

Based on the thermochronological results and modeling presented in this study, the following conclusions can be drawn for the thermotectonic evolution of the Chatkal-Kurama terrane:

1. The Chatkal-Kurama terrane records fast cooling during the Triassic-Early Jurassic (ca. 225–180 Ma) as a result of the Palaeo-Asian Ocean and the Qiangtang collision at the Eurasian margin. Subsequently, slow cooling and tectonic quiescence prevailed during the Late Jurassic-Early Cretaceous, leading to widespread denudation and marine incursion of the Paratethys.
2. Since the late Palaeogene (ca. 30 Ma), the Chatkal-Kurama terrane experienced reactivation and crustal tilting to the northwest, as a distant response to the collision of India and Eurasia and the subsequent Pamir indentation.
3. Comparing our results with the neighboring Kyrgyz western Tian Shan, the Talas-Fergana faults seemed to have acted as a structural divide, separating the low relief Chatkal-Kurama terrane from the high relief Kyrgyz Tian Shan during the Late Mesozoic.

Acknowledgments

We are grateful to Farid Divaev and Vladimir Chirikin, who were responsible for logistics and transportation in the field. As well as Andy Gleadow at the University of Melbourne for use of their Cf source. This study was supported by an Australian Research Council discovery grant (DP150101730). D. Konopelko was supported by the Ministry of Education and Science of the Russian Federation (project no. 14. Y26.31.0018) and by a travel grant (mer. 6-2018) from the Saint Petersburg State University. Ben Wade and Sarah Gilbert are thanked for assistance with the laser ablation-inductively coupled plasma-mass spectrometry facility. Ruben Rosenkranz is thanked for his constructive and thorough feedback that improved this manuscript. Data and figures supporting the conclusions presented here can be found in the supporting information. This paper forms TRaX record 408.

References

Ahmedov, N. (2000). 'Stratified and intrusive formations of Uzbekistan', *Uzbekistan Geological Survey*.

Aitchison, J. C., Ali, J. R., & Davis, A. M. (2007). When and where did India and Asia collide? *Journal of Geophysical Research*, *112*, B05423. https://doi.org/10.1029/2006JB004706

Alexeiev, D., Kröner, A., Hegner, E., Rojas-Agramonte, Y., Biske, Y., Wong, J., et al. (2016). Middle to Late Ordovician arc system in the Kyrgyz middle Tianshan: From arc-continent collision to subsequent evolution of a Palaeozoic continental margin. *Gondwana Research*, *39*, 261–291. https://doi.org/10.1016/j.gr.2016.02.003

Allen, M. B., Windley, B. F., Chi, Z., Zhong-Yan, Z., & Guang-Rei, W. (1991). Basin evolution within and adjacent to the Tien Shan range, NW China. *Journal of the Geological Society*, *148*(2), 369–378. https://doi.org/10.1144/gsjgs.148.2.0369

Bande, A., Radjabov, S., Sobel, E. R., & Sim, T. (2017). Cenozoic palaeoenvironmental and tectonic controls on the evolution of the northern Fergana basin. *Geological Society, London, Special Publications*, *427*(1), 313–335. https://doi.org/10.1144/SP427.12

Bande, A., Sobel, E. R., Mikolaichuk, A., Schmidt, A., & Stockli, D. F. (2017). Exhumation history of the western kyrgyz Tien Shan: Implications for intramontane basin formation. *Tectonics*, *36*, 163–180. https://doi.org/10.1002/2016TC004284

Bande, A., Sobel, E. R., Mikolaichuk, A., & Torres, A. V. (2017). Talas–Fergana Fault Cenozoic timing of deformation and its relation to Pamir indentation. *Geological Society, London, Special Publications*, *427*(1), 295–311. https://doi.org/10.1144/SP427.1

Bazhenov, M. L., Chauvin, A., Audibert, M., & Levashova, N. (1993). Permian and Triassic paleomagnetism of the southwestern Tien Shan: Timing and mode of tectonic rotations. *Earth and Planetary Science Letters*, *118*(1-4), 195–212. https://doi.org/10.1016/0012-821X(93)90168-9

Biske, Y., & Seltmann, R. (2010). Paleozoic Tian-Shan as a transitional region between the Rheic and Urals-Turkestan oceans. *Gondwana Research*, *17*(2-3), 602–613. The Rheic Ocean: Palaeozoic Evolution from Gondwana and Laurussia to Pangaea. Retrieved from http://www.sciencedirect.com/science/article/pii/S1342937X09002160. https://doi.org/10.1016/j.gr.2009.11.014

Bouilhol, P., Jagoutz, O., Hanchar, J. M., & Dudas, F. O. (2013). Dating the India–Eurasia collision through arc magmatic records. *Earth and Planetary Science Letters*, *366*, 163–175. https://doi.org/10.1016/j.epsl.2013.01.023

Burbank, D., McLean, J., Bullen, M., Abdrakhmatov, K., & Miller, M. (1999). Partitioning of intermontane basins by thrust-related folding, Tien Shan, Kyrgyzstan. *Basin Research*, *11*(1), 75–92. https://doi.org/10.1046/j.1365-2117.1999.00086.x

Burov, E. B., & Molnar, P. (1998). Gravity anomalies over the Ferghana Valley (central Asia) and intracontinental deformation. *Journal of Geophysical Research*, *103*(B8), 18,137–18,152. https://doi.org/10.1029/98JB01079

Burtman, V. S. (2015). Tectonics and geodynamics of the Tian Shan in the middle and late Paleozoic. *Geotectonics*, *49*(4), 302–319. https://doi.org/10.1134/S0016852115040020

Burtman, V. S., Skobelev, S. F., & Molnar, P. (1996). Late Cenozoic slip on the Talas-Ferghana fault, the Tien Shan, central Asia. *GSA Bulletin*, *108*(8), 1004–1021. https://doi.org/10.1130/0016-7606(1996)108<1004:LCSOTT>2.3.CO;2

Carrapa, B., DeCelles, P. G., Wang, X., Clementz, M. T., Mancin, N., Stoica, M., et al. (2015). Tectono-climatic implications of Eocene Paratethys regression in the Tajik basin of central Asia. *Earth and Planetary Science Letters*, *424*, 168–178. https://doi.org/10.1016/j.epsl.2015.05.034

Cawood, P. A., Kröner, A., Collins, W. J., Kusky, T. M., Mooney, W. D., & Windley, B. F. (2009). Accretionary orogens through earth history. *Geological Society, London, Special Publications*, *318*(1), 1–36. https://doi.org/10.1144/SP318.1

Clift, P. D., Carter, A., Krol, M., & Kirby, E. (2002). Constraints on India-Eurasia collision in the Arabian Sea region taken from the Indus Group, Ladakh Himalaya, India. *Geological Society, London, Special Publications*, *195*(1), 97–116. https://doi.org/10.1144/GSL.SP.2002.195.01.07

Danišík, M., Štěpančíková, P., & Evans, N. J. (2012). Constraining long-term denudation and faulting history in intraplate regions by multi-system thermochronology: An example of the Sudetic Marginal Fault (Bohemian Massif, Central Europe). *Tectonics*, *31*, TC2003. https://doi.org/10.1029/2011TC003012

De Grave, J., Buslov, M. M., & Van den haute, P. (2007). Distant effects of India–Eurasia convergence and Mesozoic intracontinental deformation in Central Asia: Constraints from apatite fission-track thermochronology. *Journal of Asian Earth Sciences*, *29*(2-3), 188–204. The 19th Himalaya-Karakoram-Tibet Workshop (HKT19) held at Niseko, Hokkaido, Japan, 10–13 July 2004. Retrieved from http://www.sciencedirect.com/science/article/pii/S136791200600071X. https://doi.org/10.1016/j.jseaes.2006.03.001

De Grave, J., Glorie, S., Buslov, M. M., Izmer, A., Fournier-Carrie, A., Batalev, V. Y., et al. (2011). The thermo-tectonic history of the Song-Kul plateau, Kyrgyz Tien Shan: Constraints by apatite and titanite thermochronometry and zircon U/Pb dating. *Gondwana Research*, *20*(4), 745–763. https://doi.org/10.1016/j.gr.2011.03.011

De Grave, J., Glorie, S., Buslov, M. M., Stockli, D. F., McWilliams, M. O., Batalev, V. Y., & et al. (2013). Thermo-tectonic history of the Issyk-Kul basement (Kyrgyz northern Tien Shan, central Asia). *Gondwana Research*, *23*(3), 998–1020. Ultrahigh-pressure and high-pressure metamorphic terranes in orogenic belts: Reactions, fluids and geological processes. Retreived from http://www.sciencedirect.com/science/article/pii/S1342937X12002377. https://doi.org/10.1016/j.gr.2012.06.014

De Grave, J., Glorie, S., Ryabinin, A., Zhimulev, F., Buslov, M., Izmer, A., et al. (2012). Late Palaeozoic and Meso-Cenozoic tectonic evolution of the southern Kyrgyz Tien Shan: Constraints from multi-method thermochronology in the Trans-Alai, Turkestan-Alai segment and the southeastern Ferghana Basin. *Journal of Asian Earth Sciences*, *44*, 149–168. Asian Climate and Tectonics. Retrieved from http://www.sciencedirect.com/science/article/pii/S1367912011001866. https://doi.org/10.1016/j.jseaes.2011.04.019

De Pelsmaeker, E., Glorie, S., Buslov, M. M., Zhimulev, F. I., Poujol, M., Korobkin, V. V., et al. (2015), Late-Paleozoic emplacement and Meso-Cenozoic reactivation of the southern Kazakhstan granitoid basement', *Tectonophysics 662*, 416–433. Special Issue on Comparative Tectonic and Dynamic Analysis of Cratons, Orogens, Basins, and Metallogeny. Retrieved from https://www.sciencedirect.com/science/article/pii/S0040195115003091, https://doi.org/10.1016/j.tecto.2015.06.014

De Pelsmaeker, E., Jolivet, M., Laborde, A., Poujol, M., Robin, C., Zhimulev, F. I., et al. (2018). Source-to-sink dynamics in the Kyrgyz Tien Shan from the Jurassic to the Paleogene: Insights from sedimentological and detrital zircon U-Pb analyses. *Gondwana Research*, *54*, 180–204. https://doi.org/10.1016/j.gr.2017.09.004

Dill, H., Kus, J., Dohrmann, R., & Tsoy, Y. (2008). Supergene and hypogene alteration in the dual-use kaolin-bearing coal deposit Angren, SE Uzbekistan. *International Journal of Coal Geology*, *75*(4), 225–240. https://doi.org/10.1016/j.coal.2008.07.003

Dolgopolova, A., Seltmann, R., Konopelko, D., Biske, Y. S., Shatov, V., Armstrong, R., et al. (2017). Geodynamic evolution of the western Tien Shan, Uzbekistan: Insights from U-Pb shrimp geochronology and Sr-Nd-Pb-Hf isotope mapping of granitoids. *Gondwana Research*, *47*, 76–109. Continental construction in central Asia and actualistic comparisons with western Pacific. Retrieved from http://www.sciencedirect.com/science/article/pii/S1342937X16304324. https://doi.org/10.1016/j.gr.2016.10.022

Donelick, R. A., & Miller, D. S. (1991). Enhanced tint fission track densities in low spontaneous track density apatites using ^{252}Cf-derived fission fragment tracks: A model and experimental observations. *International Journal of Radiation Applications and Instrumentation. Part D. Nuclear Tracks and Radiation Measurements*, *18*(3), 301–307. https://doi.org/10.1016/1359-0189(91)90022-A

Donelick, R. A., O'Sullivan, P. B., & Ketcham, R. A. (2005). Apatite fission-track analysis. *Reviews in Mineralogy and Geochemistry*, *58*(1), 49–94. https://doi.org/10.2138/rmg.2005.58.3

Dumitru, T. A., Zhou, D., Chang, E. Z., Graham, S. A., Hendrix, M. S., Sobel, E. R., & et al. (2001). Uplift, exhumation, and deformation in the Chinese Tian Shan. In M. S. Hendrix, & G. A. Davis (Eds.), *Paleozoic and Mesozoic tectonic evolution of central Asia: From continental assembly to intracontinental deformation*, (pp. 71–100). Boulder, Colorado, Memoirs-Geological Society of America.

Farley, K., Wolf, R., & Silver, L. (1996). The effects of long alpha-stopping distances on (U-Th)/He ages. *Geochimica et Cosmochimica Acta*, *60*(21), 4223–4229. https://doi.org/10.1016/S0016-7037(96)00193-7

Farley, K. A. (2002). (U-Th)/He dating: Techniques, calibrations, and applications. *Reviews in Mineralogy and Geochemistry*, *47*(1), 819–844. https://doi.org/10.2138/rmg.2002.47.18

Flowers, R. M., Farley, K. A., & Ketcham, R. A. (2015). A reporting protocol for thermochronologic modeling illustrated with data from the Grand Canyon. *Earth and Planetary Science Letters*, *432*, 425–435. https://doi.org/10.1016/j.epsl.2015.09.053

Gallagher, K. (2012). Transdimensional inverse thermal history modeling for quantitative thermochronology. *Journal of Geophysical Research*, *117*, B02408. https://doi.org/10.1029/2011JB008825

Gillespie, J., Glorie, S., Jepson, G., Zhang, Z. Y., Xiao, W. J., Danišík, M., & et al. (2017). Differential exhumation and crustal tilting in the easternmost Tianshan (Xinjiang, China), revealed by low-temperature thermochronology. *Tectonics*, *36*, 2142–2158. https://doi.org/10.1002/2017TC004574

Glorie, S., Alexandrov, I., Nixon, A., Jepson, G., Gillespie, J., & Jahn, B.-M. (2017). Thermal and exhumation history of Sakhalin Island (Russia) constrained by apatite U-Pb and fission track thermochronology. *Journal of Asian Earth Sciences*, *143*, 326–342. https://doi.org/10.1016/j.jseaes.2017.05.011

Glorie, S., & De Grave, J. (2016). Exhuming the Meso–Cenozoic Kyrgyz Tianshan and Siberian Altai-Sayan: A review based on low-temperature thermochronology. *Geoscience Frontiers*, *7*(2), 155–170. Special Issue: Exhuming Asia, https://doi.org/10.1016/j.gsf.2015.04.003

Glorie, S., De Grave, J., Buslov, M., Elburg, M., Stockli, D., Gerdes, A., & et al. (2010). Multi-method chronometric constraints on the evolution of the northern Kyrgyz Tien Shan granitoids (central Asian Orogenic Belt): From emplacement to exhumation. *Journal of Asian Earth Sciences*, *38*(3-4), 131–146. https://doi.org/10.1016/j.jseaes.2009.12.009

Glorie, S., Grave, J. D., Buslov, M. M., Zhimulev, F. I., Stockli, D. F., Batalev, V. Y., et al. (2011). Tectonic history of the Kyrgyz south Tien Shan (Atbashi-Inylchek) suture zone: The role of inherited structures during deformation-propagation. *Tectonics*, *30*, TC6016. https://doi.org/10.1029/2011TC002949

Green, P., Duddy, I., Gleadow, A., Tingate, P., & Laslett, G. (1986). Thermal annealing of fission tracks in apatite: 1. A qualitative description. *Chemical Geology: Isotope Geoscience*, *59*, 237–253. Calibration of the Phanerozoic time scale. Retrieved from http://www.sciencedirect.com/science/article/pii/0168962286900746

Green, P. F. (1986). On the thermo-tectonic evolution of northern England: Evidence from fission track analysis. *Geological Magazine*, *123*(05), 493–506. https://doi.org/10.1017/S0016756800035081

Guenthner, W. R., Reiners, P. W., Ketcham, R. A., Nasdala, L., & Giester, G. (2013). Helium diffusion in natural zircon: Radiation damage, anisotropy, and the interpretation of zircon (U-Th)/He thermochronology. *American Journal of Science*, *313*(3), 145–198. https://doi.org/10.2475/03.2013.01

Hasebe, N., Barbarand, J., Jarvis, K., Carter, A., & Hurford, A. J. (2004). Apatite fission-track chronometry using laser ablation ICP-MS. *Chemical Geology*, *207*(3-4), 135–145. https://doi.org/10.1016/j.chemgeo.2004.01.007

Hendrix, M. S., Graham, S. A., Carroll, A. R., Sobel, E. R., McKnight, C. L., Schulein, B. J., & et al. (1992). Sedimentary record and climatic implications of recurrent deformation in the Tian Shan: Evidence from Mesozoic strata of the north Tarim, south Junggar, and Turpan basins, northwest China. *GSA Bulletin*, *104*(1), 53–79. https://doi.org/10.1130/0016-7606(1992)104<0053:SRACIO>2.3.CO;2

Jepson, G., Glorie, S., Konopelko, D., Gillespie, J., Danišík, M., Evans, N. J., et al. (2018). Thermochronological insights into the structural contact between the Tian Shan and Pamirs, Tajikistan. *Terra Nova*, *30*(2), 95–104. https://doi.org/10.1111/ter.12313

Jolivet, M., Heilbronn, G., Robin, C., Barrier, L., Bourquin, S., Guo, Z., et al. (2013). Reconstructing the late Palaeozoic-Mesozoic topographic evolution of the Chinese Tian Shan: Available data and remaining uncertainties. *Advances in Geosciences*, *37*, 7–18. https://doi.org/10.5194/adgeo-37-7-2013

Kapp, P., DeCelles, P. G., Gehrels, G. E., Heizler, M., & Ding, L. (2007). Geological records of the Lhasa-Qiangtang and Indo-Asian collisions in the Nima area of central Tibet. *GSA Bulletin*, *119*(7–8), 917–933. https://doi.org/10.1130/B26033.1

Käßner, A., Ratschbacher, L., Jonckheere, R., Enkelmann, E., Khan, J., Sonntag, B., et al. (2017). Cenozoic intracontinental deformation and exhumation at the northwestern tip of the India-Asia collision—Southwestern Tian Shan, Tajikistan, and Kyrgyzstan. *Tectonics*, *35*, 2171–2194. https://doi.org/10.1002/2015TC003897

Käßner, A., Ratschbacher, L., Pfänder, J. A., Hacker, B. R., Zack, G., Sonntag, B.-L., et al. (2017). Proterozoic–Mesozoic history of the central Asian orogenic belt in the Tajik and southwestern Kyrgyz Tian Shan: U-Pb, $^{40}Ar/^{39}Ar$, and fission-track geochronology and geochemistry of granitoids. *GSA Bulletin*, *129*(3–4), 281–303. https://doi.org/10.1130/B31466.1

Konopelko, D., Klemd, R., Petrov, S., Apayarov, F., Nazaraliev, B., Vokueva, O., et al. (2017). Precambrian gold mineralization at Djamgyr in the Kyrgyz Tien Shan: Tectonic and metallogenic implications. *Ore Geology Reviews*, *86*, 537–547. https://doi.org/10.1016/j.oregeorev.2017.03.007

Konopelko, D., Seltmann, R., Mamadjanov, Y., Romer, R., Rojas-Agramonte, Y., Jeffries, T., et al. (2017), 'A geotraverse across two paleo-subduction zones in Tien Shan, Tajikistan', *Gondwana Research 47*, 110–130. Continental construction in central Asia and actualistic comparisons with western Pacific. Retrieved from http://www.sciencedirect.com/science/article/pii/S1342937X16302878. https://doi.org/10.1016/j.gr.2016.09.010

Li, S., Chung, S.-L., Wilde, S. A., Wang, T., Xiao, W.-J., & Guo, Q.-Q. (2016). Linking magmatism with collision in an accretionary orogen. *Scientific Reports*, *6*(1), 25751. https://doi.org/10.1038/srep25751

Macaulay, E. A., Sobel, E. R., Mikolaichuk, A., Kohn, B., & Stuart, F. M. (2014). Cenozoic deformation and exhumation history of the central Kyrgyz Tien Shan. *Tectonics*, *33*, 135–165. https://doi.org/10.1002/2013TC003376

McDowell, F. W., McIntosh, W. C., & Farley, K. A. (2005). A precise $^{40}Ar–^{39}Ar$ reference age for the Durango apatite (U–Th)/He and fission-track dating standard. *Chemical Geology*, *214*(3-4), 249–263. https://doi.org/10.1016/j.chemgeo.2004.10.002

Molnar, P., & Tapponnier, P. (1975). Cenozoic tectonics of Asia: Effects of a continental collision. *Science*, *189*(4201), 419–426. https://doi.org/10.1126/science.189.4201.419

Nachtergaele, S., Pelsmaeker, E. D., Glorie, S., Zhimulev, F., Jolivet, M., Danišík, M., et al. (2018). Meso-Cenozoic tectonic evolution of the Talas-Fergana region of the Kyrgyz Tien Shan revealed by low-temperature basement and detrital thermochronology. *Geoscience Frontiers*, *9*(5), 1495–1514. Special Issue: Frontiers in geoscience: A tribute to Prof. Xuanxue Mo. Retrieved from http://www.sciencedirect.com/science/article/pii/S1674987117302013. https://doi.org/10.1016/j.gsf.2017.11.007

Paton, C., Hellstrom, J., Paul, B., Woodhead, J., & Hergt, J. (2011). Iolite: Freeware for the visualisation and processing of mass spectrometric data. *Journal of Analytical Atomic Spectrometry*, *26*(12), 2508–2518. https://doi.org/10.1039/c1ja10172b

Ratschbacher, L., Hacker, B. R., Calvert, A., Webb, L. E., Grimmer, J. C., McWilliams, M. O., et al. (2003). Tectonics of the Qinling (Central China): Tectonostratigraphy, geochronology, and deformation history. *Tectonophysics*, *366*, 1), 1–1), 53.

Reiners, P. W. (2005). Zircon (U-Th)/He thermochronometry. *Reviews in Mineralogy and Geochemistry*, *58*(1), 151–179. https://doi.org/10.2138/rmg.2005.58.6

Reiners, P. W., Farley, K. A., & Hickes, H. J. (2002). He diffusion and (U–Th)/He thermochronometry of zircon: Initial results from Fish Canyon Tuff and Gold Butte. *Tectonophysics*, *349*(1-4), 297–308. Low temperature thermochronology: From tectonics to landscape evolution. Retrieved from http://www.sciencedirect.com/science/article/pii/S0040195102000586. https://doi.org/10.1016/S0040-1951(02)00058-6

Robinson, A. C. (2015). Mesozoic tectonics of the Gondwanan terranes of the Pamir plateau. *Journal of Asian Earth Sciences*, *102*, 170–179. Special Issue on Cimmerian Terranes. Retrieved from http://www.sciencedirect.com/science/article/pii/S1367912014004258. https://doi.org/10.1016/j.jseaes.2014.09.012

Samygin, S. G., & Burtman, V. S. (2009). Tectonics of the Ural paleozoides in comparison with the Tien Shan. *Geotectonics*, *43*(2), 133–151. https://doi.org/10.1134/S0016852109020058

Schwab, M., Lothar, R., Wolfgang, S., Michael, M., Vladislav, M., Valery, L., et al. (2004). Assembly of the Pamirs: Age and origin of magmatic belts from the southern Tien Shan to the southern Pamirs and their relation to Tibet. *Tectonics*, *23*, TC4002. https://doi.org/10.1029/2003TC001583

Seltmann, R., Konopelko, D., Biske, G., Divaev, F., & Sergeev, S. (2011). Hercynian post-collisional magmatism in the context of Paleozoic magmatic evolution of the Tien Shan orogenic belt. *Journal of Asian Earth Sciences*, *42*(5), 821–838. Continental accretion and intra-continental deformation of the Central Asian Orogenic Belt. Retrieved from http://www.sciencedirect.com/science/article/pii/S1367912010002646. https://doi.org/10.1016/j.jseaes.2010.08.016

Seltmann, R., & Porter, T. M. (2005). The porphyry Cu–Au/Mo deposits of Central Eurasia: 1. Tectonic, geologic and metallogenic setting and significant deposits. *Super Porphyry Copper And Gold Deposits: A Global Perspective*, *2*, 467–512.

Sobel, E. R., Chen, J., & Heermance, R. V. (2006). Late Oligocene–Early Miocene initiation of shortening in the southwestern Chinese Tian Shan: Implications for Neogene shortening rate variations. *Earth and Planetary Science Letters*, *247*(1-2), 70–81. https://doi.org/10.1016/j.epsl.2006.03.048

Sobel, E. R., & Dumitru, T. A. (1997). Thrusting and exhumation around the margins of the western Tarim basin during the India-Asia collision. *Journal of Geophysical Research*, *102*(B3), 5043–5063. https://doi.org/10.1029/96JB03267

Sobel, E. R., Oskin, M., Burbank, D., & Mikolaichuk, A. (2006). Exhumation of basement-cored uplifts: Example of the Kyrgyz range quantified with apatite fission track thermochronology. *Tectonics*, *25*, TC2008. https://doi.org/10.1029/2005TC001809

Thiede, R. C., Sobel, E. R., Chen, J., Schoenbohm, L. M., Stockli, D. F., Sudo, M., & et al. (2013). Late Cenozoic extension and crustal doming in the India-Eurasia collision zone: New thermochronologic constraints from the NE Chinese Pamir. *Tectonics*, *32*, 763–779. https://doi.org/10.1002/tect.20050

Vermeesch, P. (2009). RadialPlotter: A Java application for fission track, luminescence and other radial plots. *Radiation Measurements*, *44*(4), 409–410. https://doi.org/10.1016/j.radmeas.2009.05.003

Vermeesch, P. (2017). Statistics for LA-ICP-MS based fission track dating. *Chemical Geology*, *456*, 19–27. https://doi.org/10.1016/j.chemgeo.2017.03.002

Wagner, G., & Van den Haute, P. (1992). *Fission-track dating* (Vol. 6). New York: Springer Science & Business Media.

Windley, B. F., Alexeiev, D., Xiao, W., Kröner, A., & Badarch, G. (2007). Tectonic models for accretion of the central Asian Orogenic Belt. *Journal of the Geological Society*, *164*(1), 31–47. https://doi.org/10.1144/0016-76492006-022

Xiao, W., Windley, B. F., Allen, M. B., & Han, C. (2013). Paleozoic multiple accretionary and collisional tectonics of the Chinese Tianshan orogenic collage. *Gondwana Research*, *23*(4), 1316–1341. https://doi.org/10.1016/j.gr.2012.01.012

Xiao, W. J., Windley, B. F., Huang, B. C., Han, C. M., Yuan, C., Chen, H. L., et al. (2009). End-Permian to mid-Triassic termination of the accretionary processes of the southern Altaids: Implications for the geodynamic evolution, Phanerozoic continental growth, and metallogeny of Central Asia. *International Journal of Earth Sciences*, *98*(6), 1189–1217. https://doi.org/10.1007/s00531-008-0407-z

Zeitler, P., Herczeg, A., McDougall, I., & Honda, M. (1987). U-Th-He dating of apatite: A potential thermochronometer. *Geochimica et Cosmochimica Acta*, *51*(10), 2865–2868. https://doi.org/10.1016/0016-7037(87)90164-5